

Accepted Manuscript

Title: Hydrodynamic Performance of a Pulsed Extraction Column Containing ZnO Nanoparticles: Drop Size and Size Distribution

Authors: Pouria Amani, Mohammad Amani, R. Saidur, Wei-Mon Yan



PII: S0263-8762(17)30150-8
DOI: <http://dx.doi.org/doi:10.1016/j.cherd.2017.03.017>
Reference: CHERD 2615

To appear in:

Received date: 6-12-2016
Revised date: 4-2-2017
Accepted date: 14-3-2017

Please cite this article as: Amani, Pouria, Amani, Mohammad, Saidur, R., Yan, Wei-Mon, Hydrodynamic Performance of a Pulsed Extraction Column Containing ZnO Nanoparticles: Drop Size and Size Distribution. *Chemical Engineering Research and Design* <http://dx.doi.org/10.1016/j.cherd.2017.03.017>

This is a PDF file of an unedited manuscript that has been accepted for publication. As a service to our customers we are providing this early version of the manuscript. The manuscript will undergo copyediting, typesetting, and review of the resulting proof before it is published in its final form. Please note that during the production process errors may be discovered which could affect the content, and all legal disclaimers that apply to the journal pertain.

Hydrodynamic Performance of a Pulsed Extraction Column Containing ZnO Nanoparticles: Drop Size and Size Distribution

Pouria Amani ¹, Mohammad Amani ^{2*}, R. Saidur ^{3,4}, Wei-Mon Yan ⁵

¹ Department of Chemical Engineering, Faculty of Engineering, University of Tehran, Tehran, Iran.

² Mechanical and Energy Engineering Department, Shahid Beheshti University, Tehran, Iran.

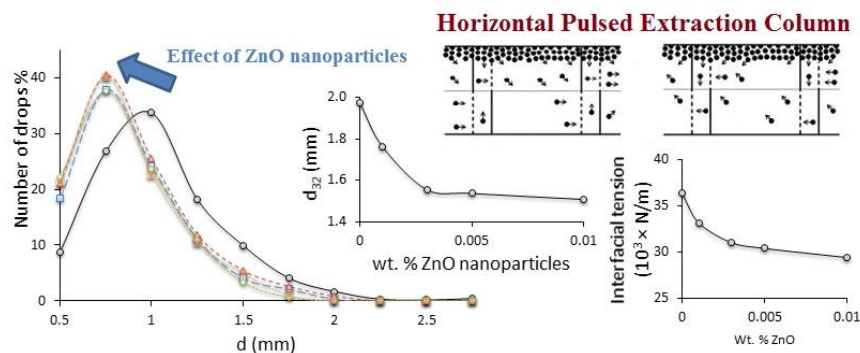
³ Faculty of Science and Technology, Sunway University, No. 5, Jalan Universiti, Bandar Sunway, 47500, Petaling Jaya, Malaysia.

⁴ Department of Engineering, Lancaster University, Lancaster, LA1 4YW, UK.

⁵ Department of Energy and Refrigerating Air-Conditioning Engineering, National Taipei University of Technology, Taipei 10608, Taiwan.

***Corresponding author:** Mohammad Amani, m_amani@sbu.ac.ir

Graphical abstract



Highlights:

- Mean drop size and size distribution is determined in a horizontal extraction column in presence of ZnO nanoparticles.
- Presence of nanoparticles reduces the interfacial tension and consequently drop sizes.
- Density of small droplets considerably increases at the first concentration of adding nanoparticles.
- The maximum entropy principle is considered for the determination of the drop size distributions.

Abstract

This article concerns the influence of different ZnO nanoparticle concentrations (0.001, 0.003, 0.005 and 0.01 wt%) along with operating parameters (i.e., pulsation intensity and flow rate of dispersed and continuous phases) and physical properties on mean drop size and drop size distribution in a horizontal pulsed perforated-plate extraction column for the toluene-acetone-water and butyl acetate-acetone-water systems (mass transfer direction from the dispersed phase to the continuous phase). According to the results, it is observed that the addition of nanoparticles has a remarkable influence on breakage and coalescence of drops and consequently their size

distribution. Accordingly, adding nanoparticles reduces the interfacial tension due to internal turbulence caused by nanoparticles' Brownian motion inside each drop. It is found that drop size distribution will shift to the left and the density of small droplets will increase in the presence of ZnO nanoparticles in the column. Furthermore, new correlation is proposed to predict mean drop size in terms of operating parameters, physical properties and nanoparticle concentration. It is also found that the maximum entropy principle is suitable to predict drop size distribution in a horizontal extraction column.

Keywords: Mean drop size; Drop size distribution; Horizontal extraction column; ZnO nanoparticles.

Nomenclature:

A	Amplitude of pulsation, m
Af	Pulsation intensity, m/s
d_{32}	Sauter mean diameter, m
f	Frequency of pulsation, Hz
g	Acceleration due to gravity, m/s ²
Q	Volumetric flow rate, m ³ /s
U	Velocity, m/s

Greek Symbols:

λ	Lagrange multipliers of probability maximum entropy function
-----------	--

μ	Viscosity, N s/m ²
ρ	Density, kg/m ³
$\Delta\rho$	Density difference between phases, kg/m ³
$\bar{\rho}$	Density of mixture of phases, kg/m ³
σ	Interfacial tension between two phases, N/m
ω	Weight fraction

Subscripts:

c	Continuous phase
d	Dispersed phase

1. Introduction

Pulsed columns are among the extractors which provide a large interfacial area using external energy input in the form of pulsing motion usually sinusoidal superimposed on counter-current flow of the liquid phases (Amani et al., 2017). One of the key parameters in the design and optimization of pulsed columns is the mean drop diameter and drop size distribution which are important in separation industries. They are directly related to the interfacial area available for mass transfer and directly affects the heat and mass transfer, stability of emulsions, rheological characteristics, reaction rate, extraction performance and final polymer particle size and properties in suspension polymerization (EL-Hamouz et al., 2009; Maaß et al., 2011; Quadros and Baptista, 2003; Yang et al., 2000). Furthermore, other parameters such as solutes, salts, surface active agents (surfactants), and nanoparticles have considerable impact on the hydrodynamic and mass transfer

performance in solvent extraction by affecting the coalescence behavior of the chemical system. Nanoparticles provide a steric hindrance around dispersed phase drops when they adsorb at the interface of two immiscible phases and form more stable dispersed phase drops against coalescence. There are many investigations on the effect of adding different nanoparticles on the enhancement of conductive and convective heat transfer coefficients (Buongiorno et al., 2009; Heris et al., 2006; Kwek et al., 2010; Lee et al., 1999; Putra et al., 2003; Wen and Ding, 2005) and several reviews are available in this field (Das et al., 2006; Yu et al., 2008). Using nanofluids offers various benefits such as stronger temperature-dependent thermal conductivity (Das et al., 2003), a substantial enhancement in the heat transfer coefficient and thermal conductivity at low nanoparticle concentration (Choi et al., 2001; Heris et al., 2006), an increment in critical heat flux in pool boiling (You et al., 2003). One of the major factors which is responsible for enhancement of heat transfer in the presence of nanoparticles is Brownian movement of nanoparticles (Amani et al., 2017a, 2017b). This mechanism similarly leads to the enhancement of mass transfer performance (Bahmanyar et al., 2011; Beiki et al., 2013a, 2013b; Jang and Choi, 2016; Keshishian et al., 2013; Krishnamurthy et al., 2006). Regarding the impact of nanoparticles on mass transfer, there are a number of studies in the literature, while most of them only investigated the convective mass transfer performance between liquid and gas phases and there have been limited investigations on the study of the presence of nanoparticles in liquid-liquid extraction which is the other popular separation process (Ashrafmansouri and Nasr Esfahany, 2015; Bahmanyar et al., 2014; Khoobi et al., 2013; Mirzazadeh Ghanadi et al., 2014; Roozbahani et al., 2014). Khoobi et al. (2013) investigated the influence of adding SiO₂ nanoparticles on droplet size and its distribution along a pulsed liquid-liquid extraction column. They revealed that addition of nanoparticles change the droplet shape from ellipsoidal to spherical. Fan et al. (2007) investigated

the impact of hydrophilic SiO₂ nanofluids on the behavior of droplets in a microchannel and a bubble column. They revealed that nanoparticles reduces the diameter of bubbles and leads to the significant reduction in holdup due to the reduction of interfacial tension. Davoodi-Nasab et al. (2013) revealed that the presence of SiO₂ nanoparticles in a mixer-settler extractor leads to the increase of holdup and the reduction of the drop size about 8.1–19.4%.

Standard vertical extraction columns meet the needs for industrial applications, but when height limitation (especially in indoor applications) are concerned it is required to use horizontal columns. It is also revealed that the mass transfer efficiency in both types of the columns is comparable (Hanson, 1971; Panahinia et al., 2017). However, considering the significant role of adding nanoparticles on hydrodynamic and mass transfer performance in a horizontal extraction column, no analytical and experimental investigation has been conducted in this regard. Therefore, this article concerns the influence of adding nanoparticles on mean drop size and drop size distribution in a horizontal pulsed perforated-plate extraction column. Mirzazadeh Ghanadi et al. (2014c) studied the impact of different nanoparticles including TiO₂, ZnO and CNT on the mass transfer performance in an extraction column. It was observed that the effect of ZnO nanoparticles on mass transfer is much greater than that of TiO₂ and CNT nanoparticles. Therefore, in this study, the influence of ZnO nanoparticles on hydrodynamic performance of the extraction column is evaluated for different liquid systems. In this work, the stability of nanofluids is firstly examined and then the effect of operating conditions and physical properties on drop size and its distribution with and without ZnO nanoparticles presence are investigated. In addition, new empirical correlations are proposed to predict the mean drop size and drop size distribution under the influence of ZnO nanoparticles.

2. Experimental

2.1. Description of the equipment

In this study, the experiments are conducted in a horizontal pulsed sieve-plate column with an internal diameter of 7 cm and length of the active area of 165 cm. The plates are half-perforated and the perforations laid on triangular pitch of 4 mm. The pulsation applies to the liquid by the pressure of air compressor and controlled by two solenoid valves. To control the liquid level in the column and regulate the discharge of heavy phase, an optical sensor in the collecting tank, in the output of the light phase, is embedded. Two rotameters are placed at the inlet of the phases to measure the flow rates. For more information, the column characteristics are listed in Table 1. A schematic of experimental setup is illustrated in Fig. 1. In addition, Fig. 2 exhibits how drops tend to move horizontally whereas the density difference drives them down or top of each compartment during the quiescent portion of the pulsation.

2.2. Liquid-liquid systems and nanofluid preparation

The chemical systems investigated in this study are toluene-acetone-water and butyl acetate-acetone-water supplied by Merck Company. The continuous phase is DI-water. Technical grade solvents of toluene and n-butyl acetate with at least 99.5 wt% purity in the presence of 3% volume fraction of acetone as a mass transfer agent ($d \rightarrow c$) are used as the dispersed phase. In order to evaluate the impact of ZnO nanoparticles on mean drop size, the experiments are carried out at four different ZnO nanoparticle concentrations (0.001, 0.003, 0.005, and 0.01 wt%). Experiments are performed in four different pulsation intensities and three different flow rates of the continuous and dispersed phases. The mass transfer direction is from the dispersed phase to the continuous phase. Physical properties of the chemical systems are listed in Table 2. The densities are determined using a scale in the order of 0.0001 g. The viscosities of both phases are measured by

a laboratory LAUDA viscometer. It should be noted that, under mass transfer conditions, a degree of uncertainty surrounds the estimation of physical properties (particularly interfacial tension), since these vary not only with the inlet solute concentrations, but also along the column. In the present research, the values of physical properties have been assumed to correspond to the mean values of acetone concentration in the continuous and dispersed phases. The mean value of acetone concentration was obtained by averaging the values obtained at the inlet and outlet of the column. In this study, the ZnO nanoparticles are supplied by US Research Nanomaterials Inc. Physical and chemical characteristics of ZnO nanoparticles are listed in Table 3. X-ray diffraction (XRD) was implemented by using an Empyrean PANalytical diffractometer to characterize the crystalline structure of the synthesized ZnO nanoparticles. The pattern is shown in Fig. 3 where a series of characteristic peaks: 2.814 (100), 2.608(002), 2.475(101), 1.911(102), 1.624(110) and 1.478(103) are observed, and they are in accordance with the zincite phase of ZnO (International Center for Diffraction Data, JCPDS 5-0664). No peaks of impurity are observed, suggesting that the high purity ZnO was obtained. Further characterization was carried out to determine the particle size distributions using dynamic light scattering (DLS) technique, which reveals the average hydrodynamic diameter of particles in a liquid suspension. Fig. 4 shows the DLS analysis for characterizing size distributions of nanoparticles. The average size (20 nm) is within the expected range of particle sizes between 15 to 30 nm.

In addition, to quantitatively determine the colloidal stability of the dispersions, the nanofluid stability was characterized using an Ultraviolet–visible spectrophotometer. Three of the considered nanoparticle concentrations (i.e., 0.001%, 0.003%, 0.005%, and 0.01%) were prepared and the time taken for sonication was about 60 min. Next, the stability of ZnO nanoparticles was evaluated by measuring the absorption of the suspensions after 8 h. According to this approach, the

absorbency of the nanofluids with different concentrations of ZnO nanoparticles was determined at 353 nm wavelength. By increasing the sediment time, the absorbance of the nanoparticles was decreased. Regarding the colloidal stability of the ZnO nanoparticles which is illustrated in Fig. 5, the relative concentration was maintained over 0.94% after 8 h compared with the initial concentrations which demonstrates the stability of the ZnO nanoparticles employed in this study. The interfacial tension of the chemical systems was determined using a Krüss tensiometer. The measured interfacial tension of the toluene-acetone-water and butyl acetate-acetone-water systems containing different amounts of ZnO nanoparticles has been shown in Fig. 6. It was obvious that by increasing ZnO concentration, interfacial tension found to be decreased, especially at low concentrations. In fact, by adding nanoparticles and increasing its concentration, interfacial tension gradually decreases due to the nanoparticles adsorption at the interface of the droplets. This reduction becomes milder with further increase in nanoparticle concentration.

2.3. Experimental procedure

All experiments were carried out at temperature $20\pm 1^\circ\text{C}$, after mutually saturating both phases before adding acetone and nanoparticles into the dispersed phase in order to avoid the excessive dissolution of the dispersed phase into the continuous phase. After dissolving the solute into the dispersed phase, the frequency and amplitude of the pulsator were next adjusted to the desired values. After filling the column with the heavy phase, the light phase was introduced. The interface location was then maintained at the desired height, and the system was allowed to reach steady state after about 90–120 min depending on the phase flow rates, pulsation intensity and the particular liquid–liquid system used. Then the drop sizes were measured by taking digital images along the column by Nikon D3100 camera in each experiment. Five inter-plate regions of active

section of the setup were chosen for capturing the photos. These regions that were equidistant from each other are pointed out in Fig. 1. It is found that the curved surface of the glass extraction column and significant differences between air and the glass refractive indices leads to a parallax deformation of the objects photographed in the extraction column. In order to omit this phenomenon, a container which filled with water was attached to the extraction column and the photographic approach was used to calculate the metal rod size of the trays holder served as the reference for the drop size measurements. Therefore, the actual size of each drop was calculated by comparison of metal rod size of the trays holder as an index with its size in the images utilizing AutoCAD software. In each image, about 300 drops were analyzed to guarantee the statistical significance of the determined Sauter mean drop diameter. Sauter-mean drop sizes were calculated using Eq. (1).

$$d_{32} = \frac{\sum_{i=1}^n n_i d_i^3}{\sum_{i=1}^n n_i d_i^2} \quad (1)$$

The observed drops had mainly spherical shapes, but in some cases ellipsoidal shapes were observed which characterized by their major axis (d_H), and their minor axis (d_L), representing the largest distance between two points on a drop and the largest length of a line, at an angle of 90° to the major axis. Accordingly, the drop diameter with an equivalent sphere was determined using Eq. (2).

$$d_i = \sqrt[3]{d_{H,i}^2 d_{L,i}} \quad (2)$$

It should be noted that measurements for Sauter-mean drop size determination were made in triplicate to verify experimental reproducibility and the obtained average data were considered for each run. Also the average absolute value of the relative deviation (AARD) was used to compare the predicted results with the experimental data. It is defined as follows:

$$AARE = \frac{1}{N} \sum_{i=1}^N \frac{|\text{Experimental value} - \text{Calculated value}|}{\text{Experimental value}} \quad (3)$$

where N is the number of points.

The experiments covered a range of dispersed and continuous phases flow rates from 2 to 8 l/h and a range of pulsation intensity (amplitude \times frequency) from 0.6 to 1.5 cm/s. Under the pulsing conditions, the rotameter was affected by the pulsation. Therefore, the flow rate of each phase was calculated by determining the volume of the liquid passed through the rotameter in 5-10 min (depending on the pulsation intensity) to ensure the accuracy of the measured flow rates. Four photos, for example, have been shown in Fig. 7, demonstrating drop sizes variations versus ZnO nanoparticle concentration.

3. Results and Discussion

3.1. Influence of adding nanoparticles

The influence of ZnO nanoparticle concentration on the mean drop size is shown in Fig. 8 at three different pulsation intensities. As shown in this figure, drop sizes decrease with augmentation of ZnO nanoparticle concentration which indicates stability of nanoparticles. According to Fig. 6, ZnO nanoparticles can reduce the interfacial tension of two chemical systems and consequently increase drop breakage, albeit not to the quantity of surfactants. In fact, nanoparticles can adsorb at the two immiscible fluids interface and consequently prevent from the coalescence of the dispersed droplets due to the fact that they provides forming 3D network or steric hindrance between drops (Aveyard et al., 2003; Binks, 2007). Therefore, as can be seen in Fig. 6, introducing the nanoparticles in the liquid-liquid system leads to the reduction in interfacial tension which results in the formation of smaller drops. Further applying nanoparticles in the system, leads to

decreasing mean drop size, although the reduction rate in d_{32} becomes slower in concentrations above 0.005 wt%, which is also achieved in a mixer-settler extractor (Raji-Asadabadi et al., 2013). In some other studies, it is also observed that the slope of mean drop size reduction is sharper at the first concentration of adding nanoparticles (Aveyard et al., 2003; Khakpay et al., 2009; Skelland and Slaymaker, 1990; Tcholakova et al., 2004). It is because of the fact that the dispersed drops reach the saturation coverage with ZnO nanoparticles when the concentration increases. Therefore, excess content of nanoparticles cannot be adsorbed at the interface and accordingly further increase in nanoparticle concentration cannot significantly influence the mean drop size. Moreover, increasing nanoparticle concentration increases the probability of sedimentation of nanoparticles. It is observed that the steeper reduction in mean drop size is achieved when the first concentration is added to liquid-liquid dispersions. On the other hand, decreasing mean drop size by adding nanoparticles does not permanently lead to the enhancement of interfacial area available for mass transfer. In fact, according to Ashrafmansouri and Nasr Esfahany (2015), at higher and lower particular nanoparticle concentrations, smaller overall mass transfer coefficient can be observed. Induced micro-convection and Brownian motion of nanoparticles are dominant in low volume fractions leading to enhanced mass transfer rate. They also revealed that deteriorated mass transfer in higher nanoparticle volume fractions is mainly because of aggregation and reduction in free volume of nanoparticles.

Fig. 8 also shows that the reduction of drop size with adding nanoparticles decreases with increment of pulsation intensity. At lower power input ($Af = 0.8$ cm/s), the decrement rate of mean drop size is 24% and 21% for toluene-acetone-water and butyl acetate-acetone-water by adding 0.01 wt% ZnO nanoparticles into the pure system. However, this reduction is about 16% and 18% respectively by dispersing same nanoparticle concentration at high power input ($Af = 1.10$ cm/s).

It can be inferred that the drop sizes are mainly influenced by agitation at high pulsation intensities and the influence of other parameters such as adding nanoparticle becomes insignificant. Similarly, this behavior is also observed for chemical systems containing surfactants as well (Khakpay et al., 2009; Tolosa et al., 2006).

3.2. Effect of Phase Flow Rates on mean drop size

The effect of dispersed and continuous phase flow rate on drop sizes with and without the presence of ZnO nanoparticles is shown in Fig. 9 and Fig. 10 respectively. It is observed that an increase in dispersed phase flow rate leads to formation of larger drops due to an increase in the number of droplets and higher coalescence rate because of consequent higher holdup (Akhgar et al., 2017). According to Fig. 10, mean drop size is directly proportional to continuous phase flow rate. This process takes place due to the reduction of slip velocity between dispersed phase droplets and the continuous phase which dominates drops coalescence in comparison with their breakage. In fact, drag forces between the droplets and the bulk continuous phase increase with incrementing the continuous phase flow rate which leads to the limitation in the drops movements and an enhancement in drops coalescence, thereby increasing mean drop size. Moreover, as can be obtained by comparing the behavior of mean drop size in two different chemical systems, the influence of phase flow rates on mean drop size in toluene-acetone-water is as strong as that in butyl acetate-acetone-water. It is also observed that the presence of nanoparticles does not significant impact on the variation of mean drop size versus phase flow rates.

3.4. Effect of the Pulsation Intensity on mean drop size

The effect of pulsation intensity on the mean drop size is shown in Fig. 11 for two liquid systems with five different concentrations of ZnO nanoparticles. The results show that mean drop size varies inversely as pulsation intensity and it declines with increment of power input in both liquid systems. This reduction is due to the intense collision of the organic phase droplets with the internals due to higher turbulence energy input and increasing Laplace pressure which causes the drops breakage to overcome their coalescence as similarly reported by Desnoyer et al. (2003) and Raji-Asadabadi et al. (2013). Furthermore, it is observed that presence of nanoparticles decreases the reduction rate of drop size versus pulsation intensity. For example, decrement rate of 25% and 18% is observed in mean drop size by varying pulsation intensity from 0.60 cm/s to 1.50 cm/s for pure toluene-acetone-water and butyl acetate-acetone-water respectively, while it is found to be about 15% and 10% for chemical systems with 0.01wt% ZnO nanoparticles.

3.5. Drop Size Distribution

The drop size distribution in pulsed sieve-plate extraction columns is mainly influenced by the interplay between drop breakage and coalescence of drops. However, it is achieved that drops breakage governs the drop size distribution in the industrially relevant operating range of pulsed extraction columns (Tsouris and Tavlarides, 1994). Since the drops are coarsely dispersed at the initial stages during experiments, the Sauter mean diameter considerably declines in the direction of the flow rate of the dispersed phase as a result of frequent breakage at sieve plates, tending to a constant value. Moreover, it is seen that the drop size distributions are broader in the initial stages, becoming narrower and shifting towards smaller drop sizes along the column until a steady-state distribution is achieved. Regarding the evaluation of drop size distribution and irrespective of

different nanoparticle contents, the influence of operating parameters (i.e., pulsation intensity and dispersed and continuous phase flow rates) on drop size distribution is illustrated in Fig. 12 and 13 for toluene-acetone-water and butyl acetate-acetone-water respectively. It is found that drop size distribution shifts to the left and small droplets densities increases with an increment in pulsation intensity due to the fact that smaller drops form narrower and more homogeneous distributions because of presence of smaller eddies in liquid systems (Chen and Middleman, 1967). Moreover, it is observed that the influence of power input overrides the effect of interfacial tension at high pulsation intensity which results in similar drop size distribution in both chemical systems in identical conditions, although the interfacial tension has considerable impact on the shape of the distribution curves at lower pulsation intensity. It is generally revealed that in the absence of pulsation, interfacial tension and buoyancy are the cause of the drop breakup (Kumar and Hartland, 1996; Yadav and Patwardhan, 2008), while in the presence of pulsation, a smaller drop size is formed, and the drop size distribution is less spread out in higher pulsation as a consequence of an intensified collision between the drops and the internal plates and the internal wall, which causes a higher breakage rate (Gholam Samani et al., 2012; Khajenoori et al., 2015; Ousmane et al., 2011; Usman et al., 2009).

According to Fig. 14 and Fig. 15, an increase in dispersed phase flow rates leads to wider drop size distribution because of higher coalescence rate, while the continuous phase flow rate has negligible impact on drop size distribution which is probably because of low breakage frequency. It is also reported by previous investigators that more easily coalescence of drops will take place in liquid-liquid systems with higher interfacial tension (Treybal, 1981).

The effect of different nanoparticle concentrations on the drop size distribution for two different chemical systems is shown in Fig. 14 at pulsation intensity of 0.95 cm/s and dispersed and continuous phase flow rates of 2 and 4 l/h, respectively. From this figure, an interesting observation can be made. An increment in power input increases the small droplet densities more remarkable for chemical systems in the presence of nanoparticles compared to those for pure systems. It is also observed that drop size distributions in different nanoparticle concentrations are not significantly distinctive and are almost similar. However, since drops size distribution is found to be narrower for 0.01% in both chemical systems, it can be obtained that more nanoparticle concentrations can lead to more droplet breakage which can be referred to the internal turbulence caused by the nanoparticles Brownian motion inside each drop which is believed to intensify drop breakage (Krishnamurthy et al., 2006). In some studies, it is reported that the influence of interfacial tension is significantly high on drops coalescence that can be considered as the only affecting factor (Bikerman, 2013; Oppermann, 1941).

3.6. Predictive Correlation for Mean Drop Size

Regarding the prediction of mean drop size, the following correlation is proposed in terms of operating parameters including pulsation intensity and dispersed and continuous phase flow rate, physical properties of chemical systems and weight fraction of nanoparticles by dimensional analysis methods using SPSS software:

$$\frac{d_{32}}{\sqrt{\frac{\gamma}{\Delta\rho g}}} = 3.41 \times 10^{-5} \left(\frac{Af}{U_d}\right)^{-0.243} \left(\frac{\Delta\rho}{\rho_c}\right)^{-1.637} \left(\frac{\mu_c}{\mu_d}\right)^{0.112} \left(\frac{\mu_d U_d}{\gamma}\right)^{-0.152} \times \left(1 + \frac{U_d}{U_c}\right)^{-0.074} (1 + \omega)^{-0.565} \quad (4)$$

where g represents acceleration due to gravity (m/s^2), Af represents pulsation intensity, ρ and μ denote the density and viscosity of each phase, and U is the superficial velocity of each phase. The influence of nanoparticle concentration is considered by ω which represents the weight fraction of nanoparticles. The comparison of experimental data with those calculated by Eq. (4) is illustrated in Fig. 15. This figure shows the accuracy of the derived equation to predict mean drop sizes. The AARE for Eq. (4) is found to be about 7.47%.

3.7. Prediction Correlation for Drop Size Distribution

Many researchers have proposed a number of probability distribution functions for prediction of drop size distribution in liquid-liquid extraction systems that were shown in Table 4. The probability density has been taken into consideration as the ratio of number of drops with a specific diameter to the total number of drops which is called number density. In these methods, a non-linear regression analysis is required to fit the theoretical distribution functions and to determine α and β parameters.

However, maximum entropy approach is another method which is recently developed in order to evaluate drop size distribution in extraction columns and it is found that maximum entropy method has better predictive ability to predict experimental data (Asadollahzadeh et al., 2017, 2016, 2015). Therefore, this method is considered in order to predict drop size distribution in the column which can be expressed as follows:

$$P_n(d) = \exp(-\lambda_0 - \lambda_1 f_1^2(d_i) - \lambda_2 f_2^3(d_i)) \quad (5)$$

where λ_0 , λ_1 and λ_2 are Lagrange multipliers which have to be determined for each particular solution. The following constraints for drops size distribution can be defined:

$$S = -k \int_0^{\infty} P \ln(P) d(d) \quad (6)$$

$$\int_0^{\infty} P f_k d(d) = F_k \quad (7)$$

$$\int_0^{\infty} P_n(d) d(d) = 1 \quad (8)$$

$$\int_0^{\infty} P_n(d) d^3 d(d) = d_{30}^3 \quad (9)$$

$$\int_0^{\infty} P_n(d) d^2 d(d) = \frac{d_{30}^3}{d_{32}} \quad (10)$$

Based on the abovementioned constraints, the Lagrange multipliers are determined and consequently the probability drop diameter distribution can be achieved in terms of operating parameters including pulsation intensity and low rate of dispersed and continuous phase, physical properties of liquid-liquid systems and weight fraction of nanoparticles. The following correlation is obtained:

$$\lambda_i = C_1 \left(\frac{Af}{U_d} \right)^{C_2} \left(\frac{\Delta\rho}{\rho_c} \right)^{C_3} \left(\frac{\mu_c}{\mu_d} \right)^{C_4} \left(\frac{\mu_d U_d}{\gamma} \right)^{C_5} \left(1 + \frac{U_d}{U_c} \right)^{C_6} (1 + \omega)^{C_7} \quad (11)$$

The values of constant parameters, C_1 to C_7 in Eq. (11), are presented in Table 5. Regarding the AARE of Eq. (11), it can be obtained that maximum entropy approach has a good predictive ability to determine drop size distribution in a horizontal extraction column and satisfactory agreement between experimental and calculated data has been observed.

4. Conclusions

In this study, mean drop size and drop size distribution in a horizontal pulsed sieve-plate extraction column is investigated for toluene-acetone-water and butyl acetate-acetone-water (mass transfer direction from dispersed to continuous phase) with dispersing 0.001, 0.003, 0.005 and 0.01 wt% ZnO nanoparticle concentrations into the dispersed phase in order to evaluate the effect of presence of nanoparticles on drops behavior. It was observed that addition of various contents of nanoparticles leads to the reduction of mean drop size due to the decrement of interfacial tension. In fact, the Brownian motion of nanoparticles inside dispersed drops intensify drops breakage which results in internal turbulence, thereby decreasing interfacial tension. Accordingly, applying nanoparticles shifts drop size distributions to the left and increases the density of small droplets as well. Furthermore, regarding better understanding the influence of affecting parameters on drop size and its distribution, an empirical correlation is proposed for predicting the mean drop size as a function of the operating variables, the physical properties of the system, and concentration of the nanoparticles with an Average Absolute Relative Error (AARE) of 7.47%. For prediction of drop size distribution, the maximum entropy principle is found to be able to estimate the experimental data with satisfactory agreement. The AARE of the Lagrange multipliers in this regard are from 7.48% to 8.95%.

REFERENCES

- Akhgar, S., Safdari, J., Towfighi, J., Amani, P., Mallah, M.H., 2017. Experimental investigation on regime transition and characteristic velocity in a horizontal–vertical pulsed sieve-plate column. *RSC Adv.* 7, 2288–2300.
- Amani, M., Amani, P., Kasaeian, A., Mahian, O., Kasaeian, F., Wongwises, S., 2017a. Experimental study

- on viscosity of spinel-type manganese ferrite nanofluid in attendance of magnetic field. *J. Magn. Magn. Mater.* 428, 457–463.
- Amani, M., Amani, P., Kasaeian, A., Mahian, O., Wongwises, S., 2017b. Thermal conductivity measurement of spinel-type ferrite MnFe_2O_4 nanofluids in the presence of a uniform magnetic field. *J. Mol. Liq.* 230, 121–128.
- Amani, P., Safdari, J., Abolghasemi, H., Mallah, M.H., Davari, A., 2017. Two-phase pressure drop and flooding characteristics in a horizontal-vertical pulsed sieve-plate column. *Int. J. Heat Fluid Flow.* doi:10.1016/j.ijheatfluidflow.2017.01.003
- Asadollahzadeh, M., Torab-Mostaedi, M., Shahhosseini, S., Ghaemi, A., 2015. Using maximum entropy approach for prediction of drop size distribution in a pilot plant multi-impeller extraction contactor. *Rsc Adv.* 5, 95967–95980.
- Asadollahzadeh, M., Torab-Mostaedi, M., Torkaman, R., Safdari, J., 2016. A new model for prediction of drop size distribution in a liquid–liquid extraction column. *RSC Adv.* 6, 82496–82504.
- Asadollahzadeh, M., Torkaman, R., Torab-Mostaedi, M., Safdari, J., 2017. A comparison between drop size distributions derived from the probability distribution functions and maximum entropy principle. Case study; pilot plant Scheibel extraction column. *Chem. Eng. Res. Des.* 117, 648–658.
- Ashrafmansouri, S.-S., Nasr Esfahany, M., 2015. The influence of silica nanoparticles on hydrodynamics and mass transfer in spray liquid–liquid extraction column. *Sep. Purif. Technol.* 151, 74–81.
- Aveyard, R., Binks, B.P., Clint, J.H., 2003. Emulsions stabilised solely by colloidal particles. *Adv. Colloid Interface Sci.* 100–102, 503–546.
- Bahmanyar, A., Khoobi, N., Moharrer, M.M.A., Bahmanyar, H., 2014. Mass transfer from nanofluid drops in a pulsed liquid-liquid extraction column. *Chem. Eng. Res. Des.* 92, 2313–2323.
- Bahmanyar, A., Khoobi, N., Mozdianfard, M.R., Bahmanyar, H., 2011. The influence of nanoparticles on hydrodynamic characteristics and mass transfer performance in a pulsed liquid-liquid extraction column. *Chem. Eng. Process. Process Intensif.* 50, 1198–1206.
- Beiki, H., Esfahany, M.N., Etesami, N., 2013a. Turbulent mass transfer of Al_2O_3 and TiO_2 electrolyte

- nanofluids in circular tube. *Microfluid. Nanofluidics* 15, 501–508.
- Beiki, H., Esfahany, M.N., Etesami, N., 2013b. Laminar forced convective mass transfer of γ - Al_2O_3 /electrolyte nanofluid in a circular tube. *Int. J. Therm. Sci.* 64, 251–256.
- Bikerman, J., 2013. *Surface chemistry: theory and applications*. Elsevier.
- Binks, B.P., 2007. Colloidal particles at liquid interfaces. *Phys. Chem. Chem. Phys.* 9, 6298.
- Buongiorno, J., Venerus, D.C., Prabhat, N., McKrell, T., Townsend, J., Al., E., 2009. A benchmark study on the thermal conductivity of nanofluids. *J. Appl. Phys.* 106, 94312.
- Chen, H.T., Middleman, S., 1967. Drop size distribution in agitated liquid-liquid systems. *AIChE J.* 13, 989–995.
- Choi, S.U.S., Zhang, Z.G., Yu, W., Lockwood, F.E., Grulke, E.A., 2001. Anomalous thermal conductivity enhancement in nanotube suspensions. *Appl. Phys. Lett.* 79, 2252–2254.
- Das, S.K., Choi, S.U.S., Patel, H.E., 2006. Heat Transfer in Nanofluids—A Review. *Heat Transf. Eng.* 27, 3–19.
- Das, S.K., Putra, N., Thiesen, P., Roetzel, W., 2003. Temperature dependence of thermal conductivity enhancement for nanofluids. *J. Heat Transfer* 125, 567–574.
- Davoodi-Nasab, P., Abolghasemi, H., Safdari, J., Raji-Asadabadi, M., 2013. Study on the simultaneous effect of silica nanoparticles and cetyl trimethyl ammonium bromide on drop size in mixer-settler extractor. *J. Taiwan Inst. Chem. Eng.* 44, 854–862.
- Desnoyer, C., Masbernat, O., Gourdon, C., 2003. Experimental study of drop size distributions at high phase ratio in liquid-liquid dispersions. *Chem. Eng. Sci.* 58, 1353–1363.
- EL-Hamouz, A., Cooke, M., Kowalski, A., Sharratt, P., 2009. Dispersion of silicone oil in water surfactant solution: Effect of impeller speed, oil viscosity and addition point on drop size distribution. *Chem. Eng. Process. Process Intensif.* 48, 633–642.
- Fan, L.S., Hemminger, O., Yu, Z., Wang, F., 2007. Bubbles in nanofluids. *Ind. Eng. Chem. Res.* 46, 4341–4346.
- Gholam Samani, M., Haghighi Asl, A., Safdari, J., Torab-Mostaedi, M., 2012. Drop size distribution and

- mean drop size in a pulsed packed extraction column. *Chem. Eng. Res. Des.* 90, 2148–2154.
- Hanson, C., 1971. *Recent Advances In Liquid-Liquid Extraction*. Elsevier.
- Heris, S.Z., Etemad, S.G., Esfahany, M.N., 2006. Experimental investigation of oxide nanofluids laminar flow convective heat transfer. *Int. Commun. Heat Mass Transf.* 33, 529–535.
- Jang, S.P., Choi, S.U.S., 2016. Role of Brownian motion in the enhanced thermal conductivity of nanofluids. *Appl. Phys. Lett.* 4316, 19–22.
- Keshishian, N., Nasr Esfahany, M., Etesami, N., 2013. Experimental investigation of mass transfer of active ions in silica nanofluids. *Int. Commun. Heat Mass Transf.* 46, 148–153.
- Khajenoori, M., Haghighi-Asl, A., Safdari, J., Mallah, M.H., 2015. Prediction of drop size distribution in a horizontal pulsed plate extraction column. *Chem. Eng. Process. Process Intensif.* 92, 25–32.
- Khakpay, A., Abolghasemi, H., Salimi-Khorshidi, A., 2009. The effects of a surfactant on mean drop size in a mixer-settler extractor. *Chem. Eng. Process. Process Intensif.* 48, 1105–1111.
- Khoobi, N., Bahmanyar, A., Molavi, H., Bastani, D., Mozdianfard, M.R., Bahmanyar, H., 2013. Study of droplet behaviour along a pulsed liquid-liquid extraction column in the presence of nanoparticles. *Can. J. Chem. Eng.* 91, 506–515.
- Krishnamurthy, S., Bhattacharya, P., Phelan, P.E., Prasher, R.S., 2006. Enhanced mass transport in nanofluids. *Nano Lett.* 6, 419–423.
- Kumar, A., Hartland, S., 1996. Unified Correlations for the Prediction of Drop Size in Liquid-Liquid Extraction Columns. *Ind. Eng. Chem. Res.* 35, 2682–2695.
- Kwek, D., Crivoi, A., Duan, F., 2010. Effects of Temperature and Particle Size on the Thermal Property Measurements of Al_2O_3 - Water Nanofluids. *J. Chem. Eng. Data* 55, 5690–5695.
- Lee, S., Choi, S.U.S., Li, S., Eastman, J.A., 1999. Measuring Thermal Conductivity of Fluids Containing Oxide Nanoparticles. *J. Heat Transfer* 121, 280–289.
- Maaß, S., Wollny, S., Voigt, A., Kraume, M., 2011. Experimental comparison of measurement techniques for drop size distributions in liquid/liquid dispersions. *Exp. Fluids* 50, 259–269.

- Mirzazadeh Ghanadi, A., Heydari Nasab, A., Bastani, D., Seife Kordi, A.A., 2014. The Effect of Nanoparticles on the Mass Transfer in Liquid–Liquid Extraction. *Chem. Eng. Commun.* 202, 600–605.
- Moreira, É., Pimenta, L.M., Carneiro, L.L., Faria, R.C.L., Mansur, M.B., Ribeiro, JR, C.P., 2005. Hydrodynamic Behavior of a Rotating Disc Contactor Under Low Agitation Conditions. *Chem. Eng. Commun.* 192, 1017–1035.
- Oppermann, R.H., 1941. Emulsions and foams. *J. Franklin Inst.* 232, 389–390
- Ousmane, S., Isabelle, M., Mario, M.S., Mamadou, T., Jacques, A., 2011. Study of mass transfer and determination of drop size distribution in a pulsed extraction column. *Chem. Eng. Res. Des.* 89, 60–68.
- Panahinia, F., Ghannadi-Maragheh, M., Safdari, J., Amani, P., Mallah, M.-H., 2017. Experimental investigation concerning the effect of mass transfer direction on mean drop size and holdup in a horizontal pulsed plate extraction column. *RSC Adv.* 7, 8908–8921.
- Putra, N., Roetzel, W., Das, S.K., 2003. Natural convection of nano-fluids. *Heat Mass Transf. und Stoffuebertragung* 39, 775–784.
- Quadros, P.A., Baptista, C.M.S.G., 2003. Effective interfacial area in agitated liquid-liquid continuous reactors. *Chem. Eng. Sci.* 58, 3935–3945.
- Raji-Asadabadi, M., Abolghasemi, H., Maragheh, M.G., Davoodi-Nasab, P., 2013. On the mean drop size of toluene/water dispersion in the presence of silica nanoparticles. *Chem. Eng. Res. Des.* 91, 1739–1747.
- Rinconrubio, L., Kumar, A., Hartland, S., 1994. Drop-Size Distribution and Average Drop Size in a Wirz Extraction Column. *Chem. Eng. Res. Des.* 72, 493–502.
- Roobahani, M.A.G., Najafabadi, M.S., Abadi, K.N.H., Bahmanyar, H., 2014. Simultaneous Investigation of the Effect of Nanoparticles and Mass Transfer Direction on Static and Dynamic Holdup in Pulsed-Sieve Liquid–Liquid Extraction Columns. *Chem. Eng. Commun.* 202, 1468–1477.
- Skelland, a. H.P., Slaymaker, E. a., 1990. Effects of surface-active agents on drop size in liquid-liquid

- systems. *Ind. Eng. Chem. Res.* 29, 494–499.
- Tcholakova, S., Denkov, N.D., Banner, T., 2004. Role of surfactant type and concentration for the mean drop size during emulsification in turbulent flow. *Langmuir* 20, 7444–7458.
- Tolosa, L., Forgiarini, A., Moreno, P., Salager, J., 2006. Combined Effects of Formulation and Stirring on Emulsion Drop Size in the Vicinity of Three-Phase Behavior of Surfactant–Oil Water Systems. *Ind. Eng. Chem. Res.* 45, 3810–3814.
- Treybal, R.E., 1981. *Mass-transfer operations*. New York 784.
- Tsouris, C., Tavlarides, L.L., 1994. Breakage and Coalescence Model for Drops in Turbulent Dispersion. *AIChE J.* 40, 395–406.
- Tung, L.S., Luecke, R.H., 1986. Mass transfer and drop sizes in pulsed-plate extraction columns. *Ind. Eng. Chem. Process Des. Dev.* 25, 664–673.
- Usman, M.R., Sattar, H., Hussain, S.N., Muhammad, H., Asghar, A., Afzal, W., 2009. Drop size in a liquid pulsed sieve-plate extraction column. *Brazilian J. Chem. Eng.* 26, 677–683.
- Wen, D., Ding, Y., 2005. Experimental investigation into the pool boiling heat transfer of aqueous based γ -alumina nanofluids. *J. Nanoparticle Res.* 7, 265–274.
- Yadav, R.L., Patwardhan, A.W., 2008. Design aspects of pulsed sieve plate columns. *Chem. Eng. J.* 138, 389–415.
- Yang, B., Takahashi, K., Takeishi, M., 2000. Styrene Drop Size and Size Distribution in an Aqueous Solution of Poly(vinyl alcohol). *Ind. Eng. Chem. Res.* 39, 2085–2090.
- You, S.M., Kim, J.H., Kim, K.H., 2003. Effect of nanoparticles on critical heat flux of water in pool boiling heat transfer. *Appl. Phys. Lett.* 83, 3374–3376.
- Yu, W., France, D.M., Routbort, J.L., Choi, S.U.S., 2008. Review and Comparison of Nanofluid Thermal Conductivity and Heat Transfer Enhancements. *Heat Transf. Eng.* 29, 432–460.

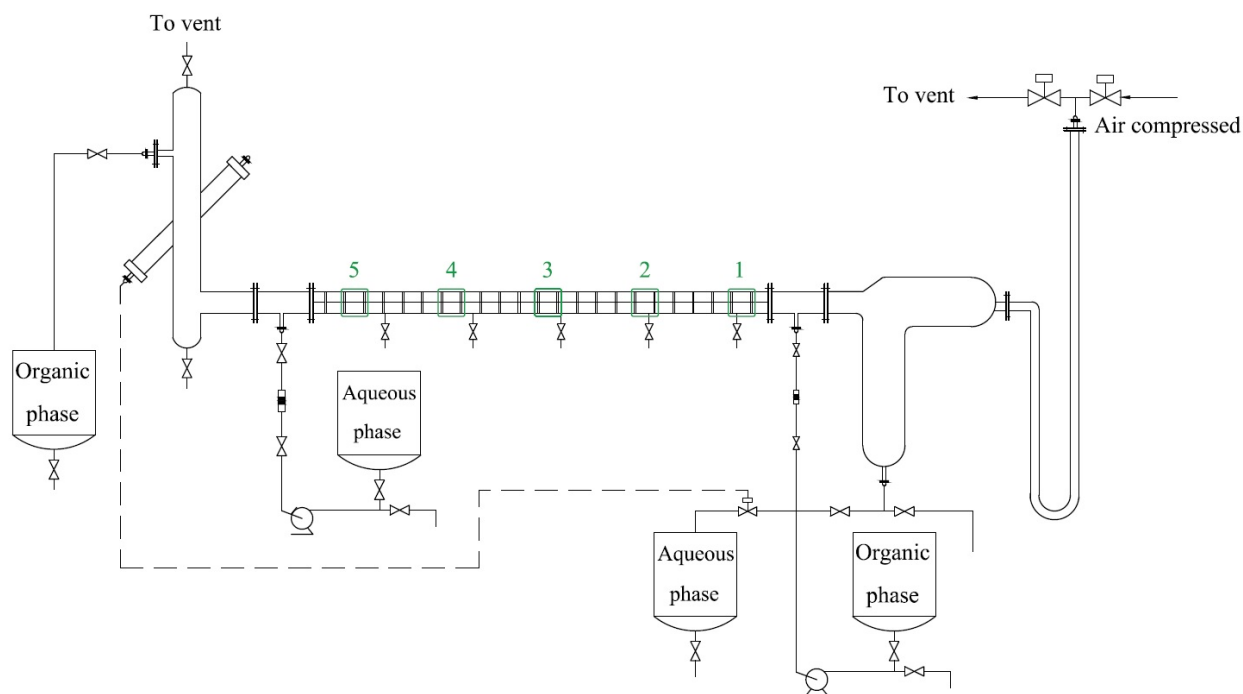


Figure 1. A schematic diagram of the horizontal pulsed sieve plate column. Points 1 to 5 indicate the inter-plate regions of the column chosen for capturing the photos.

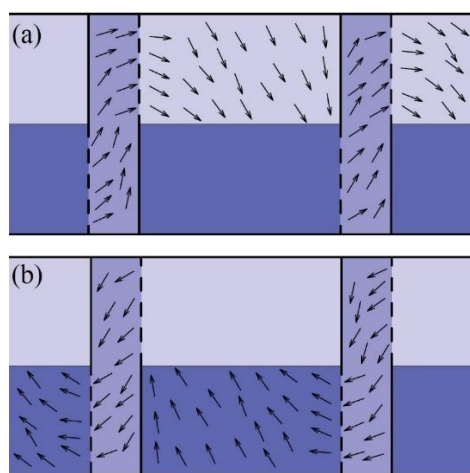


Figure 2. Drops movement in each compartment during the quiescent portion of the pulsation (a) Left to right stroke and (b) Right to left stroke

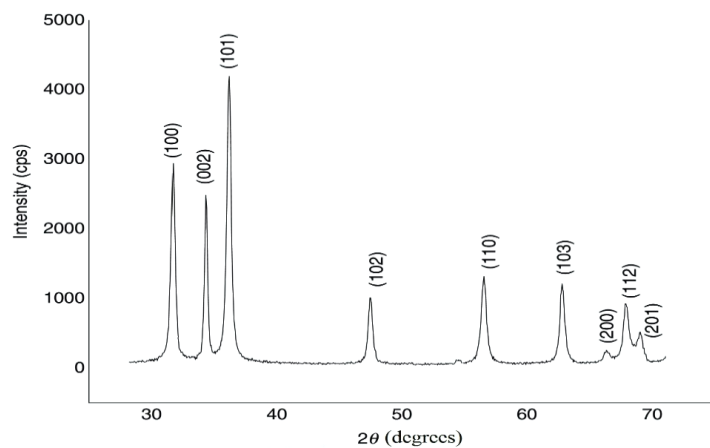


Figure 3. XRD pattern of ZnO nanoparticles

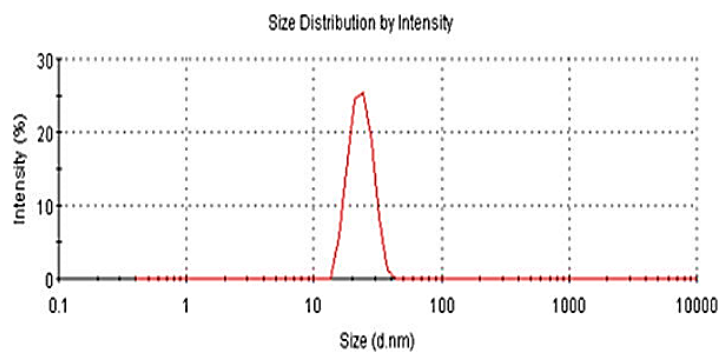


Figure 4. Particle size distribution of ZnO nanoparticles

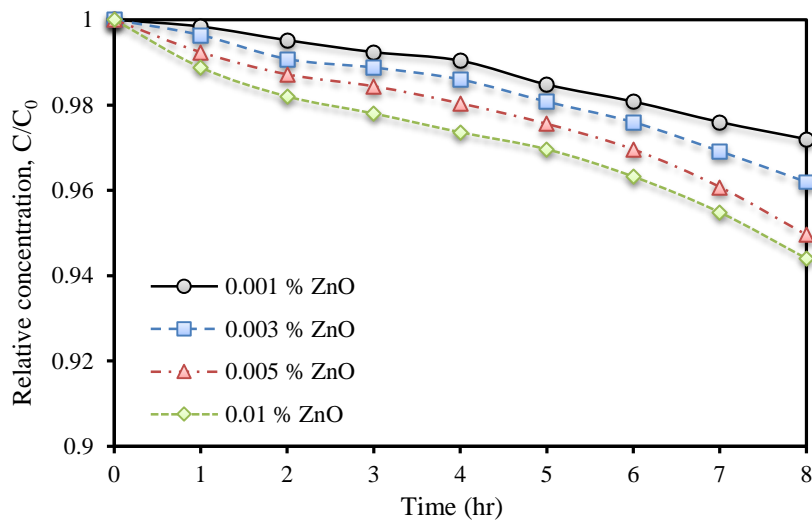


Figure 5. Relative supernatant concentration of ZnO nanoparticles as a function of the elapsed time for 0.001, 0.003, 0.005, and 0.01 wt% of ZnO nanoparticles

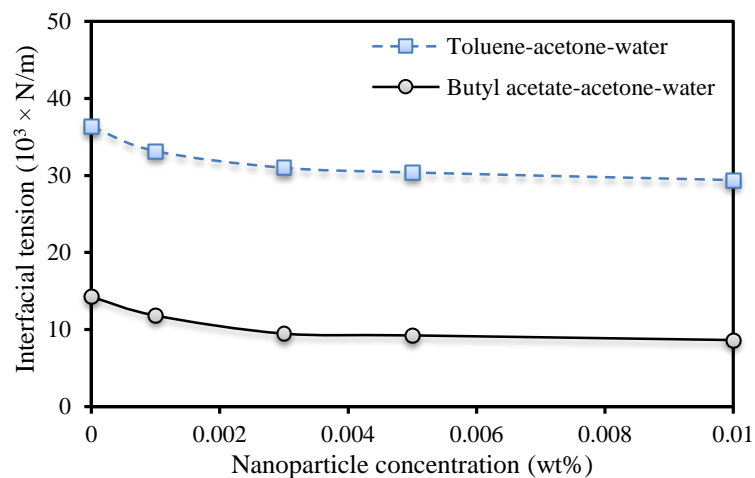
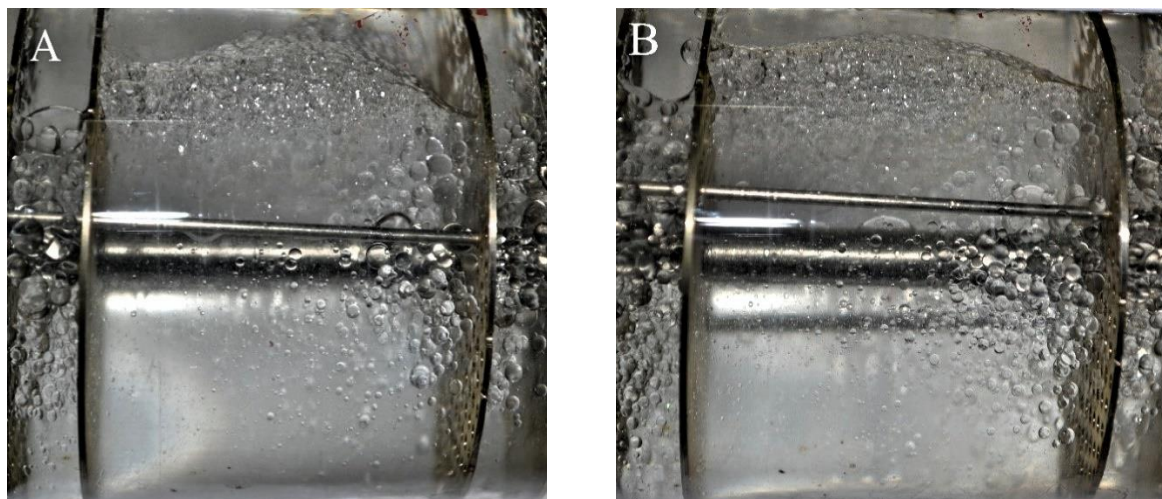


Figure 6. Interfacial tensions variation versus ZnO concentrations for toluene-acetone-water and butyl acetate-acetone-water



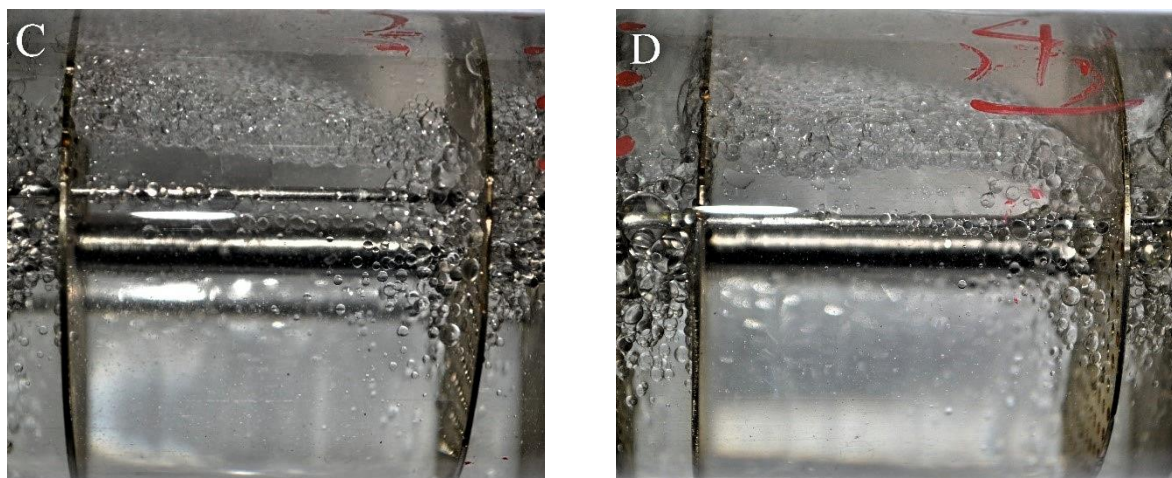


Figure 7. Four photos taken due to drops at $Af = 0.8$ cm/s, $Q_d = 2$ L/h and $Q_c = 4$ L/h. (A) 0.001 wt%, (B) 0.003 wt%, (C) 0.005 wt%, and (D) 0.01 wt%

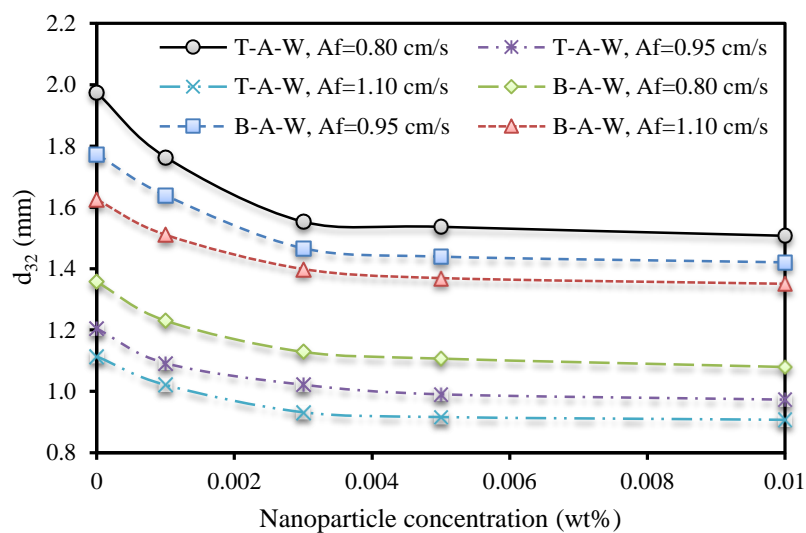


Figure 8. Influence of ZnO nanoparticle concentration on mean drop size at constant pulsation intensity of 1.1 cm/s, dispersed phase flow rate of 2 l/h and continuous phase flow rate of 6 l/h for toluene-acetone-water (T-A-W) and butyl acetate-acetone-water (B-A-W).

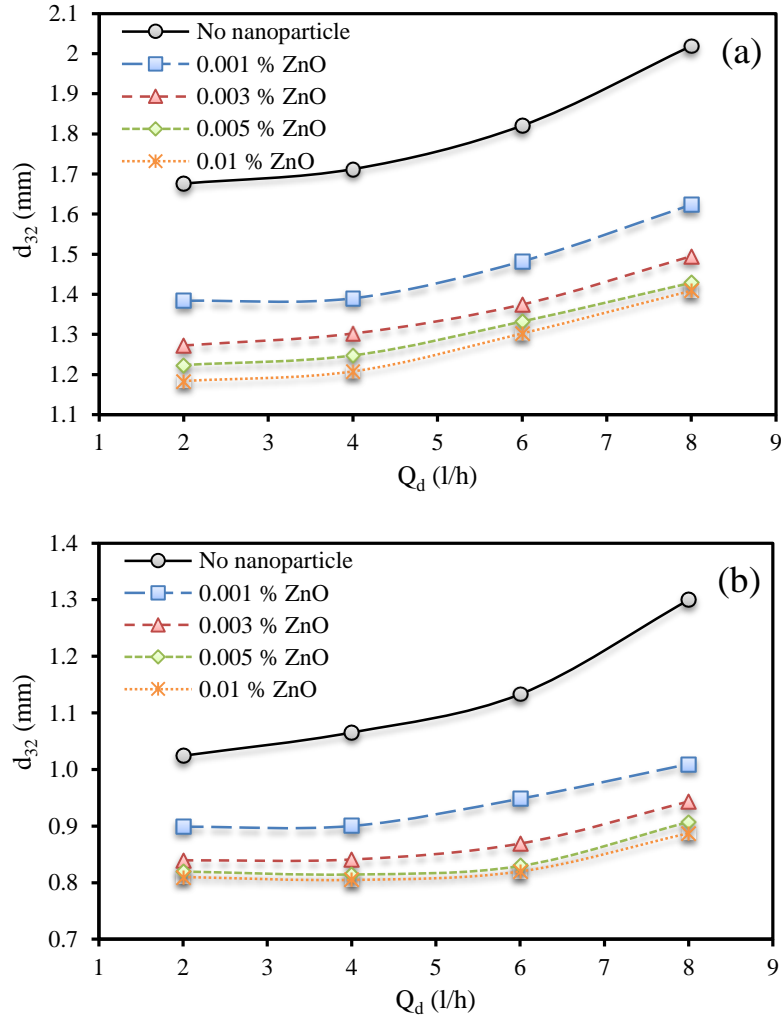


Figure 9. Influence of the continuous phase flow rate on mean drop size for (a) toluene-acetone-water and (b) butyl acetate-acetone-water at constant pulsation intensity of 0.8 cm/s and dispersed phase flow rate of 4 l/h for different nanoparticle concentrations.

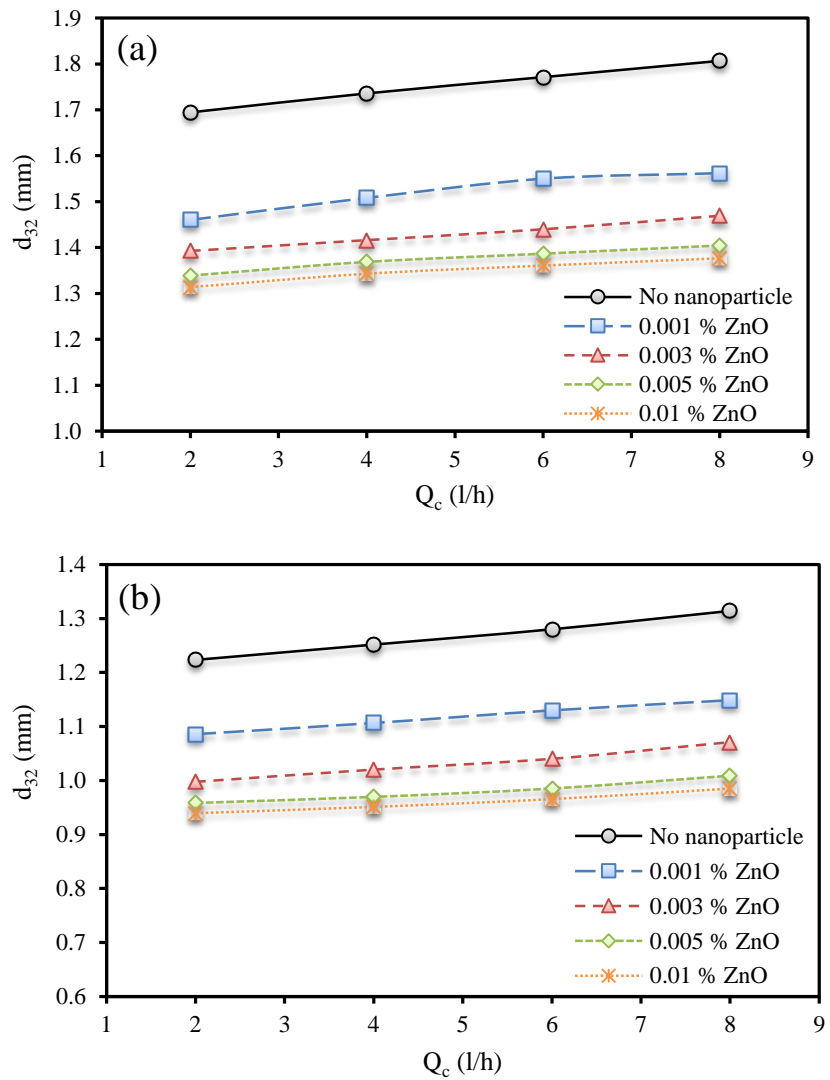


Figure 10. Influence of the dispersed phase flow rate on mean drop size for (a) toluene-acetone-water and (b) butyl acetate-acetone-water at constant pulsation intensity of 1.1 cm/s and continuous phase flow rate of 6 l/h for different nanoparticle concentrations.

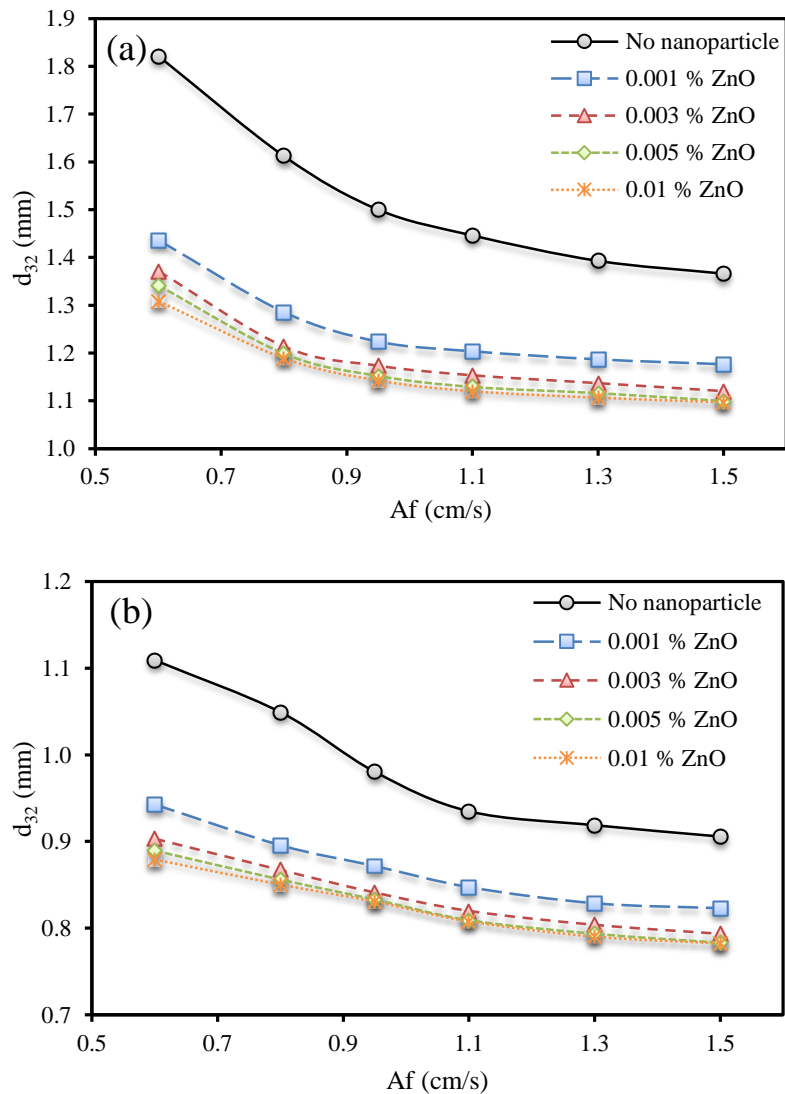


Figure 11. Influence of the pulsation intensity on mean drop size at constant dispersed and continuous phase flow rate of 4 and 6 l/h for (a) toluene-acetone-water and (b) butyl acetate-acetone-water for different nanoparticle concentrations.

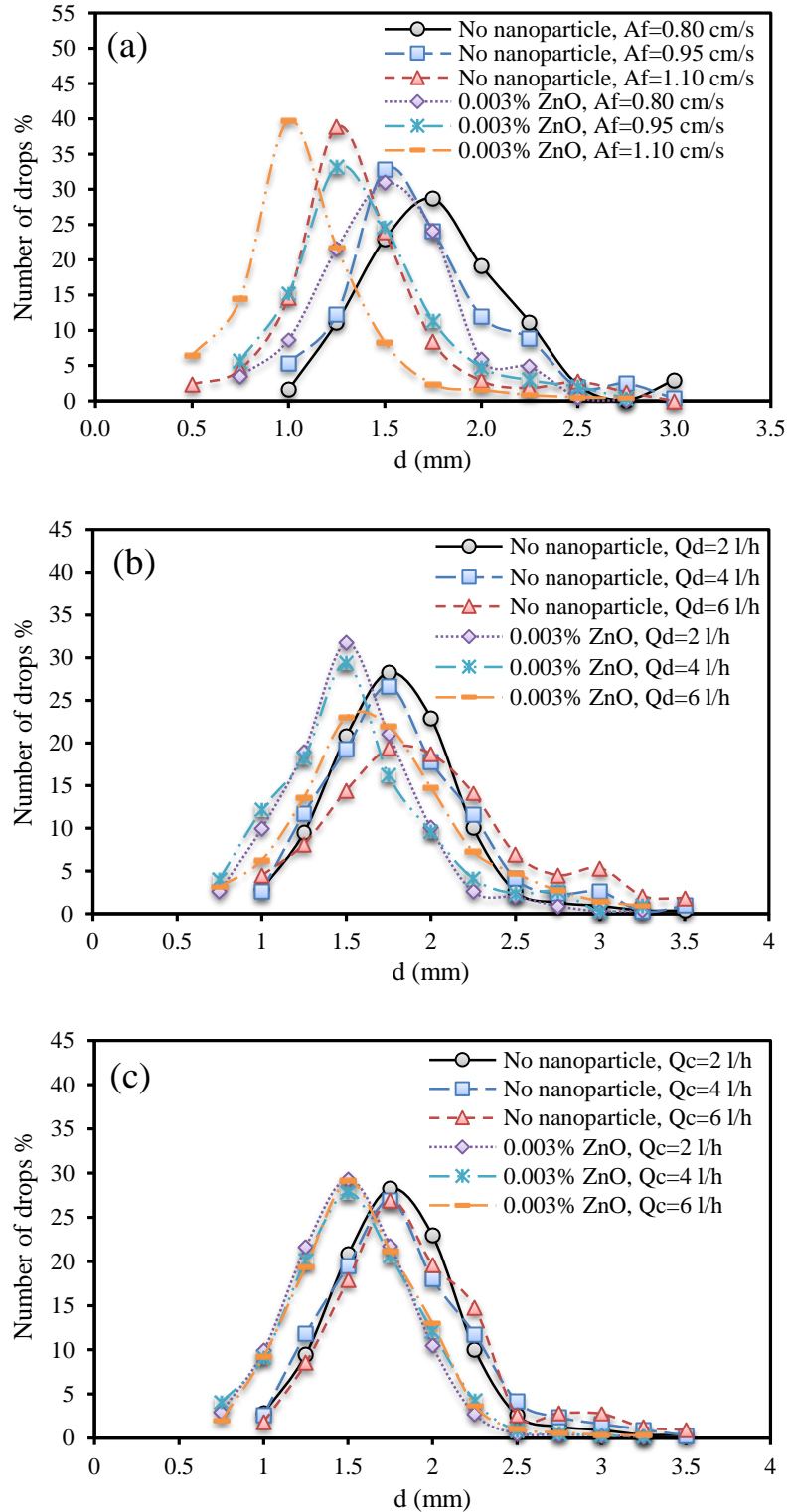


Figure 12. Influence of (a) pulsation intensity at constant phase flow rate of 2 l/h, (b) dispersed phase flow rate at constant pulsation intensity of 0.80 cm/s and continuous phase flow rate of 2 l/h and (c) continuous phase flow rate at constant pulsation intensity of 0.80 cm/s and continuous phase flow rate of 2 l/h

phase flow rate at constant pulsation intensity of 0.80 cm/s and dispersed phase flow rate of 2 l/h on drop size distribution for toluene-acetone-water.

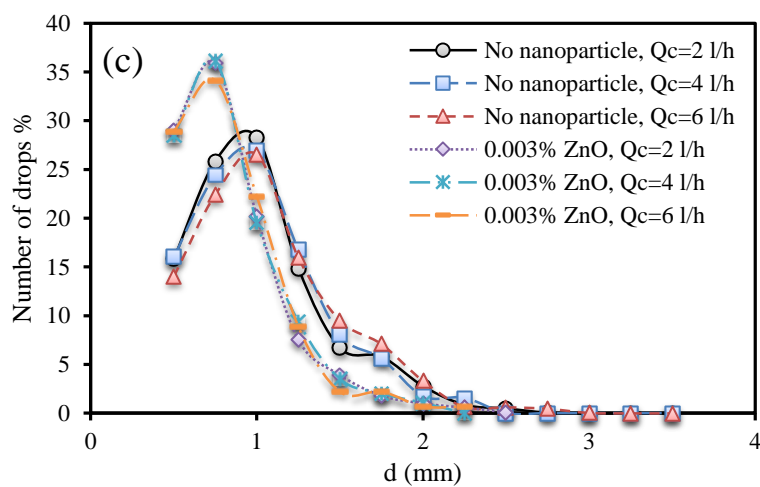
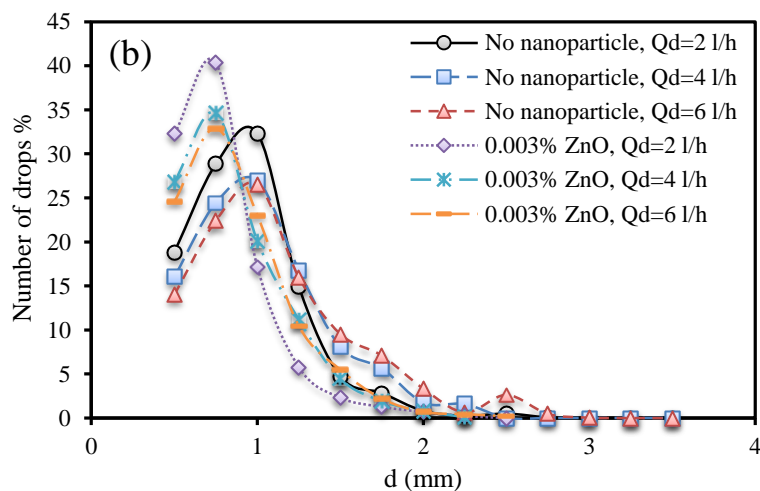
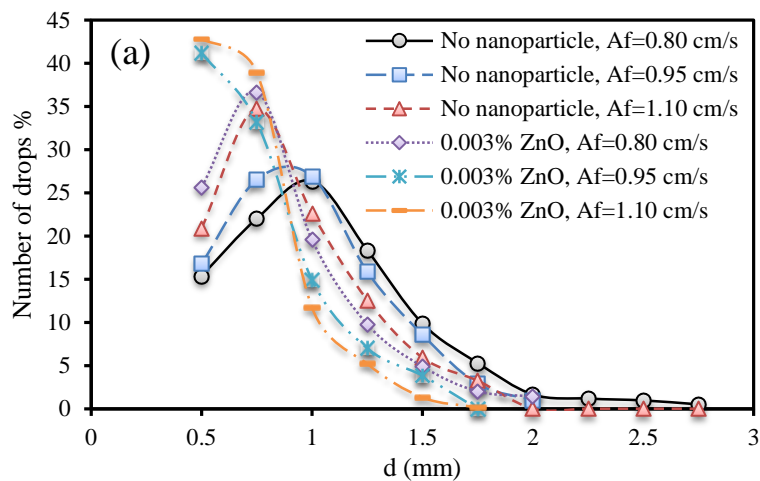


Figure 14 Influence of (a) pulsation intensity at constant phase flow rate of 2 l/h, (b) dispersed phase flow rate at constant pulsation intensity of 0.80 cm/s and continuous phase flow rate of 2 l/h and (c) continuous phase flow rate at constant pulsation intensity of 0.80 cm/s and dispersed phase flow rate of 2 l/h on drop size distribution for butyl acetate-acetone-water

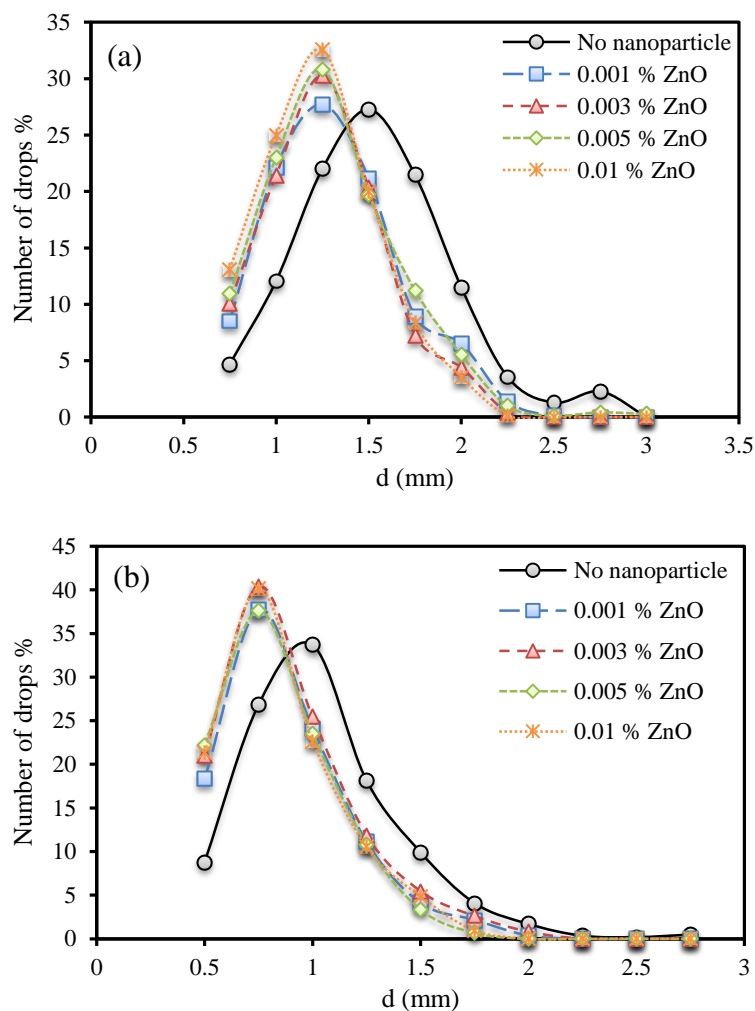


Figure 14. Influence of presence of ZnO nanoparticles on drop size distribution in different concentrations for (a) toluene-acetone-water and (b) butyl acetate-acetone-water.

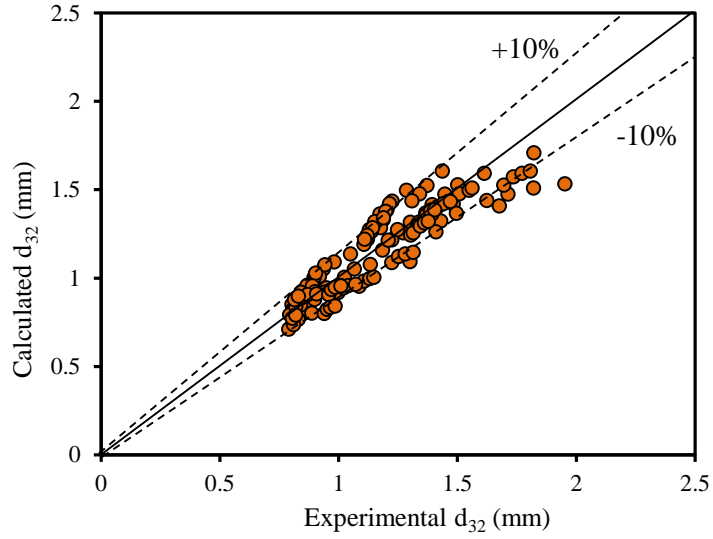


Figure 15. Comparison of experimental data and those obtained from Eq. (4).

Table 1. Geometrical characteristics of the column used

Material of construction the column	glass
Material used for plates, spacers and rod	Stainless steel
Column length (m)	1.65
Column diameter (cm)	7
Upper and lower settler diameter (cm)	9
Upper settler length (cm)	50
Lower settler length (cm)	50
Holes pitch (mm)	4
Holes diameter (mm)	2

Plates thickness (mm)	1
Plate spacing (cm)	1* , 6**
Average free area of the plates (%)	0.11

* spacing between two individual plates in a pair

** spacing between two pairs in a cell

Table 2. Properties of systems used

Chemical systems	Toluene-acetone-water (T-A-W)			Butyl acetate-acetone-water (B-A-W)		
Physical properties	ρ kg/m ³	μ mPa.s	γ mN/m	ρ kg/m ³	μ mPa.s	γ mN/m
Organic phase	865	0.579	36.1	881	0.68	14.4
Aqueous phase	995	1.17		997	1.14	

Table 3. Properties of ZnO nanoparticles

Parameter	Value
Purity	> 99%
Diameter	10 - 30 nm
Density	5.606 g/cm ³
Color	White
Morphology	Nearly spherical
Crystal phase	Single crystal

Table 4. Probability distribution functions for liquid–liquid extraction systems.

Name	Function	Reference
Normal	$P_n(d) = \frac{1}{\sqrt{2\pi}\alpha} \exp\left[-\left(\frac{d-\beta}{\sqrt{2}\alpha}\right)^2\right]$	(Moreira et al., 2005)

Log-normal	$P_n(d) = \frac{1}{\sqrt{2\pi d \alpha}} \exp\left[-\left(\frac{\ln d - \beta}{\sqrt{2\alpha}}\right)^2\right]$	(Moreira et al., 2005)
Log-normal	$P_n(d) = \frac{\alpha}{d\sqrt{\pi}} \exp\left[-\left(\alpha \ln \frac{d}{dq}\right)^2\right]$	(Rinconrubio et al., 1994)
Gamma	$P_n(d) = \frac{\beta}{\Gamma(\alpha+1)} d^\alpha \exp(-\beta d)$	(Rinconrubio et al., 1994)
Weibull	$P_n(d) = \alpha \beta d_i^{\alpha-1} \exp(-\beta d_i^\alpha)$	(Tung and Luecke, 1986)

Table 5. Constant parameters and AARE values for λ_i in maximum entropy approach.

Maximum entropy approach	C ₁	C ₂	C ₃	C ₄	C ₅	C ₆	C ₇	%AARE
λ_0	1.51	-0.63	-0.42	-0.56	-0.446	0	0	7.48
λ_1	-91.5	-0.79	3.76	0.81	0.57	0	0	8.95
λ_2	156.7	2.44	8.83	1.79	2.16	0.69	4.52	8.16